

**Manuscript version: Published Version**

The version presented in WRAP is the published version (Version of Record).

**Persistent WRAP URL:**

<http://wrap.warwick.ac.uk/166450>

**How to cite:**

The repository item page linked to above, will contain details on accessing citation guidance from the publisher.

**Copyright and reuse:**

The Warwick Research Archive Portal (WRAP) makes this work of researchers of the University of Warwick available open access under the following conditions.

© 2022 Optica Publishing Group under the terms of the [Optica Open Access Publishing Agreement](#)


**Publisher's statement:**

Please refer to the repository item page, publisher's statement section, for further information.

For more information, please contact the WRAP Team at: [wrap@warwick.ac.uk](mailto:wrap@warwick.ac.uk).



# Broadband high-gain Yb: YAG crystal-derived silica fiber for low noise tunable single-frequency fiber laser

YING WAN,<sup>1</sup> JIANXIANG WEN,<sup>1,\*</sup> CHEN JIANG,<sup>1</sup>  FENGZAI TANG,<sup>2</sup> TAXIMAITI YUSUFU,<sup>3</sup> FUFEI PANG,<sup>1</sup> AIERKEN SIDIKE,<sup>3</sup> AND TINGYUN WANG<sup>1</sup>

<sup>1</sup>Key Lab of Specialty Fiber Optics and Optical Access Networks, Joint International Research Laboratory of Specialty Fiber Optics and Advanced Communication, School of Communication and Information Engineering, Shanghai University, 99 Shangda Road, Shanghai 200444, China

<sup>2</sup>WMG, University of Warwick, Coventry, CV4 7AL, UK

<sup>3</sup>Xinjiang Key Laboratory for Luminescence Minerals and Optical Functional Materials, School of Physics and Electronic Engineering, Xinjiang Normal University, Urumqi, Xinjiang 830054, China

\*wenjx@shu.edu.cn

**Abstract:** An over 75 nm broadband spectrum with a gain per unit length of  $>2$  dB/cm was obtained from a homemade Yb: YAG crystal-derived silica fiber (YCDSF) with Yb-doping concentration of 6.57 wt.%. Using a 13-cm-long YCDSF, a low-noise wavelength-tunable single-frequency fiber laser has been constructed, enabling a single longitudinal mode oscillation from 1009 to 1070 nm. In particular, in the 1023-1056 nm waveband, the laser operating at any wavelength exhibited a maximum output power over 37 mW with power fluctuations below 0.38%, a slope efficiency  $>8\%$ , and an optical signal-to-noise ratio higher than 60 dB. A linewidth of less than 2.8 kHz was also observed at the maximum pump powers, and relative intensity noise was as low as -155 dB/Hz at frequencies above 1.0 MHz. These results indicate that the YCDSFs with broadband high-gain characteristics are promising for wavelength-tunable fiber lasers in applications such as optical coherence tomography, precision metrology, nonlinear frequency conversion, and so on.

© 2022 Optica Publishing Group under the terms of the [Optica Open Access Publishing Agreement](#)

## 1. Introduction

Since the advent of Cr: YAG crystal-derived fibers [1] in 2006, YAG crystal-derived silica fibers have received extensive attention due to their excellent properties in low photodarkening effect [2], high rare-earth-ion doping concentration [3], high thermal conductivity, and high stimulated Brillouin scattering threshold [4]. To date, a number of crystals or ceramics derived silica fibers have been fabricated using the melt-in-tube method, such as Ce/Tb: YAG [5], Nd: YAG [6,7], Yb: YAG [3,8–15], Er: YAG [16,17], Tm: YAG [18,19], and so on. The operating wavelengths of these fibers cover from visible light to mid-infrared, and the corresponding application fields range from radiation detection to single-frequency fiber lasers (SFFLs) and ultrafast fiber lasers. It is noted that Yb: YAG crystal-derived silica fiber (YCDSF) shows a low transmission loss and a high gain per unit length, which greatly improves the performance of  $\sim 1$   $\mu\text{m}$  waveband SFFLs. In 2019, Xie et al [10,11] developed the YCDSF using the secondary drawing method, whose transmission loss was reduced to 0.5 dB/m. Based on this fiber, a high-power lasing output of 6 W and a single-frequency lasing output of 110 mW have been obtained. In 2020, our group greatly increased the Yb doping concentration in YCDSF using the drawing technique heated by a CO<sub>2</sub> laser, so that the YCDSF gain coefficient reached 4.4 dB/cm. An over 255 mW single-longitudinal-mode (SLM) laser was achieved using a 0.7-cm-long YCDSF [14]. At the same time, a ring-cavity SFFL with a narrow linewidth has been demonstrated using

YCDSF, and its maximum output power and slope efficiency also were up to 100 mW and 18.3% respectively [15]. In addition to low loss and high gain, the YCDSF also exhibits broadband amplified spontaneous emission (ASE). Due to the amorphized nature of fiber core in YCDSF, the characteristic emission of  $\text{Yb}^{3+}$  ion is significantly broadened, and its emission cross-section covers the 900 to 1110 nm waveband [14]. Moreover, the high Yb doping concentration in the fiber core makes the reabsorption effect more obvious, which further widens the ASE spectrum, e.g. 800-1400 nm waveband for a 10-cm YCDSF [20]. These merits associated with YCDSF suggest that it could be suitable for applications in tunable fiber lasers and ultrafast fiber lasers, which are yet to be exploited.

At the same time, various applications in spectroscopy, medicine, optical communication, optical instrument, and scientific research [21–23] rely on wavelength-tunable fiber lasers. In particular, wavelength-tunable single-frequency fiber lasers (TSFFLs), are driven by the applications in biomedicine for optical coherence tomography, precision metrology, molecular spectroscopy, and nonlinear frequency conversion systems [24–27]. This is because that TSFFLs have remarkable performance in low noise, narrow linewidth, high coherence, and high stability. To obtain the tunable single-frequency lasing, a ring-cavity laser comprising a tunable bandpass filter (TBF) and a section of unpumped Yb-doped fiber is an efficient way. Based on this kind of laser cavity, several studies have been conducted using commercial Yb-doped fibers [28–33]. The obtained laser output performances are however inferior to those of single-wavelength SFLLs, in terms of the output power, slope efficiency, and relative intensity noise (RIN). At the same time, meter-scale gain fibers had to be utilized in ring-cavity TSFFLs to provide sufficient gain, which led to a reduction in the longitudinal mode spacing of the laser. The bandwidth narrowing effect of the induced grating based on commercial Yb-doped fibers is also limited, making the laser prone to mode hopping [15]. These constraints could directly undermine the resolution, sensitivity, and stability of the optical detection, sensing, and imaging systems where the TSFFLs are deployed. Therefore, high-performance TSFFLs put forward higher requirements on gain fibers, in terms of gain coefficient and bandwidth.

In this work, a bandwidth high-gain YCDSF was introduced to construct a ring-cavity TSFFL, whose performances were evaluated in terms of wavelength-tunable range, output power, noise, and so on.

## 2. Yb: YAG crystal-derived silica fiber and ring-cavity TSFFL construction

The YCDSF was fabricated using the melt-in-tube method. In this case, the preform of the YCDSF consisted of a commercially available 15.0 at% Yb: YAG crystal rod, and a high-purity silica substrate tube. The Yb: YAG crystal rod was 3-cm-long with a diameter of 1.9-mm. The inner and outer diameters of the silica tube were 2-mm and 20-mm, respectively. The fiber pulling speed and the feeding speed are 1.0 m/min and 0.04 mm/min, respectively. A more detailed fabrication process was reported in our previous works [13–15]. The concentration of Yb ions in the core region, obtained using an electron probe micro-analyzer (EPMA-1720, SHIMADZU, Japan), was approximately 6.57 wt.%. The core and cladding diameters were 9.5 and 125.2  $\mu\text{m}$ , respectively. The absorption spectrum of the YCDSF investigated using the cut-back method, is depicted in Fig. 1(a). The background loss of the fiber was  $\sim 0.7$  dB/m at 1100 nm. Two absorption peaks at 924.1 and 976.2 nm are observed. The absorption coefficient was up to 43.2 dB/cm at 976.2 nm. The high absorption coefficient is attributed to the high  $\text{Yb}^{3+}$  ions doping concentration, revealing that this fiber can be effectively pumped by the 976 nm laser. Figure 1(b) shows the ASE spectra of a 2-cm-long YCDSF with different pump powers of a 976 nm laser. Intensive and broadband ASE spectra are observed in the wavelength range of 900 to 1200 nm, originating from  $\text{Yb}^{3+}$  ions. With the increase in the pump power, the intensity of the ASE increases gradually. Especially, the 20 dB bandwidths of the ASE were up to 127 nm. Furthermore, the gain coefficient was characterized at different signal wavelengths and powers,

as presented in Fig. 1(c). As the signal light power increased, the corresponding gain coefficient decreased at a given signal wavelength. Simultaneously, the gain coefficient initially increased and then decreased with the increase in the signal light wavelength. Its maximum gain coefficient reached 6.1 dB/cm at 1025 nm. The intensity distribution of the gain coefficient with the signal power of -20 dBm is analyzed in Fig. 1(d), which is consistent with the ASE spectral shape of the YCDSF. The gain change trend is mainly determined by the luminescence properties of  $\text{Yb}^{3+}$  ions in YCDSF. These results indicate that the fabricated YCDSF in this work is an excellent candidate for use in the applications of broadband ASE light sources and broadband tunable lasers.

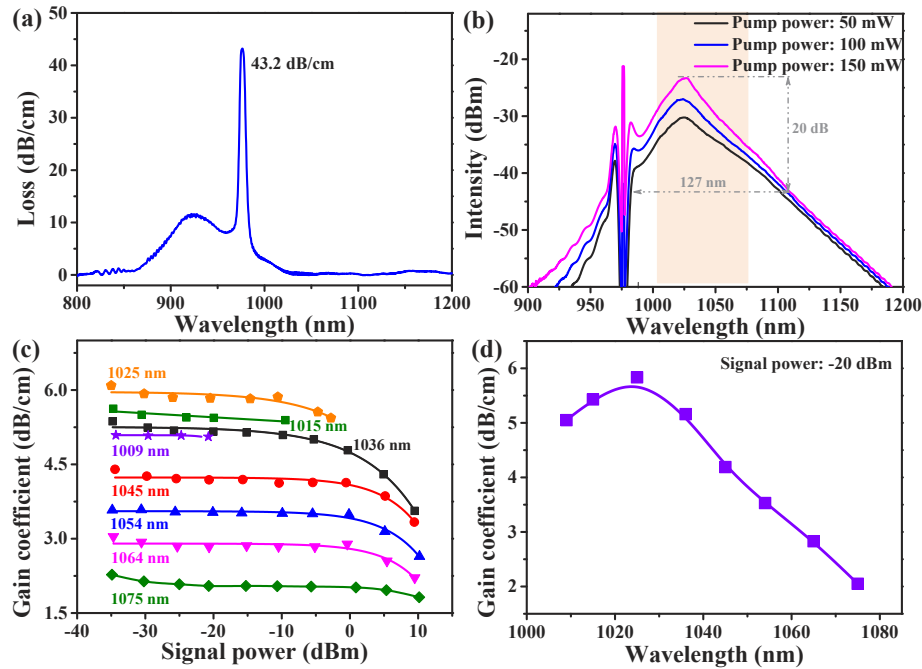


**Fig. 1.** The absorption spectrum of the YCDSF (a); ASE spectra of the fiber with different pump powers (b); Gain coefficient of the fiber at different wavelengths (c); Gain coefficient spectrum of the fiber with -20 dBm signal power (d).

Figure 2 illustrated the ring-cavity TSFFL with a forward core-pumping scheme and its associated measurement system. The laser system consists of two kinds of home-made Yb-doped silica fibers, a 980/1030 nm wave-plate single-mode wavelength division multiplexer (WDM), an optical circulator (CIR), two 3 dB single-mode couplers (OCs), and a TBF (WLTfNM-P-1060-60-SM-FC, Micro Photons Technology Co., China). Here, a 980 nm fiber laser was connected to the ring cavity through the WDM as a pumping source. A 13-cm-long YCDSF was used as the gain fiber. A low concentration Bi/Er/Yb co-doped silica fiber was used as a saturable absorber (SA) to form a narrowband induced grating [15]. The two output ports of the OC were connected as a loop mirror. The insertion loss of the CIR was approximately 3.5 dB in the range of 1010-1070 nm. Its function is to introduce the induced grating and ensure unidirectional transmission of the signal light. The 3 dB bandwidth and tunable range of the TBF were 0.5 nm and 60 nm, respectively. Another OC, as an output port, was spliced with the CIR and TBF. A polarization controller was employed to adjust the polarization states of the signal light to facilitate the formation of stable standing waves. The laser output can be selectively connected to either an optical spectrum analyzer (OSA, 70, Yokogawa, Japan), a power meter (PM, PM100D,

Thorlabs, USA), or an electrical spectrum analyzer (ESA, R&S, Agilent, Germany), depending on the requirements.

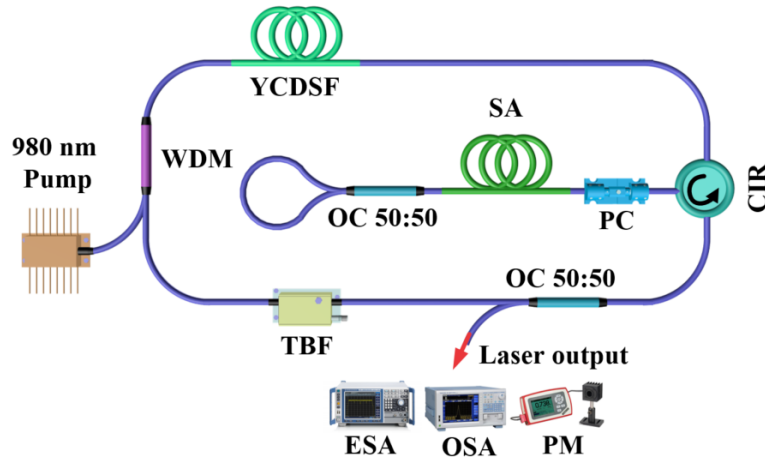


**Fig. 2.** Experimental setup of the ring-cavity TSFFL and laser measurement system (WDM, wavelength-division multiplexer; OC, coupler; SA, saturable absorber; PC, polarization controller; CIR, circulator; TBF, tunable bandpass filter; ESA, electric spectrum analyzer; OSA, optical spectrum analyzer; PM, power meter).

To gain insights into the SLM operation, a theoretical analysis was performed on the longitudinal mode interval ( $\Delta\nu$ ) of the ring-cavity laser and the bandwidth of induced grating ( $\Delta\nu$ ). The  $\Delta\nu$  depends only on the cavity length of the laser. Without insertion of a SA fiber, the cavity length of the laser was 5.22 m. When a section of SA fiber was added,  $\Delta\nu$  changed with the length of the SA fiber, as depicted by the red curve in Fig. 3. As the length of the SA fiber was increased from 0 to 10.0 m,  $\Delta\nu$  was reduced from 39.4 to 9.9 MHz.  $\Delta\nu$  is mainly determined by the properties of the Bi/Er/Yb co-doped silica fiber. We chose a Bi/Er/Yb co-doped silica fiber as the SA fiber in light of two aspects as explained next. First, it has a low Yb ions doping concentration. The number of Yb ions per unit volume is approximately  $0.13 \times 10^{26}$  ions/m<sup>3</sup> ( $0.32 \times 10^{26}$  ions/m<sup>3</sup> for

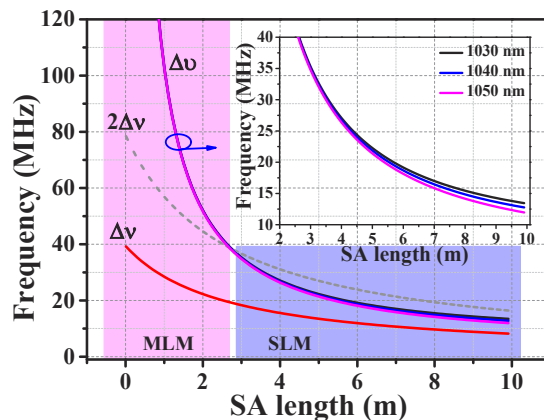


**Fig. 3.** Calculated longitudinal mode spacing ( $\Delta\nu$ ) and bandwidth of the induced grating ( $\Delta\nu$ ) as a function of the SA fiber length (MLM, multiple-longitudinal-mode; SLM, single-longitudinal-mode).

a commercial Yb-doped fiber [34]), which leads to a smaller emission cross-section at  $\sim 1.0 \mu\text{m}$  wavebands. Next, the energy transfer of co-doped ions from  $\text{Yb}^{3+}$  ions to  $\text{Er}^{3+}$  ions and bismuth active centers [35], may also play a role, resulting in the reduced emission cross-section of Yb ions.  $\Delta\nu$  is proportional to the emission cross-section of the SA fiber [15,36], which suggests that the Bi/Er/Yb co-doped silica fiber is a promising SA fiber to form a narrowband induced grating. The changing trend of  $\Delta\nu$  at different wavelengths was further estimated as a function of the length of the SA fiber, as plotted by the black (1030 nm), blue (1040 nm), and pink (1050 nm) curves in Fig. 3. The inset shows an enlarged view for the SA fiber length range of 2.0 to 10.0 m, where  $\Delta\nu$  decreased with the red shift of the working wavelength. The condition  $\Delta\nu \leq 2\Delta\nu$  should be satisfied to obtain SLM operation ( $2\Delta\nu$ , as shown by the gray curve in Fig. 3). The critical length of the SA fiber is approximately 2.8 m. When the length of the SA fiber is larger than the critical value, the laser is more likely to achieve SLM operation, as indicated by the purple rectangular area in Fig. 3. Different SA fiber lengths (4.0, 6.0, and 8.0 m) were tested experimentally and the 4.0 m fiber length demonstrated the best performances in terms of maximum output power, slope efficiency, and optical signal-to-noise (OSNR). Therefore, we focus on the performances of the TSFFL with a 4.0-m SA fiber.

### 3. Evaluation of the tunable ring-cavity single-frequency fiber lasers

The tunable performance of the fiber laser was demonstrated by adjusting the operating wavelength of the TBF. The output spectra of the TSFFL were measured by an OSA with a resolution of 0.02 nm, as illustrated in Fig. 4(a). The wavelength tuning range was 1009-1070 nm (up to 61 nm) at a pump power of 680 mW. Its tuning range may be limited mainly by the self-oscillation laser and the working wavelength of the TBF and CIR. A lower OSNR was observed at a shorter or longer working wavelength, mainly owing to the intensity distributions of the ASE of  $\text{Yb}^{3+}$  ions. The spontaneous emission probability of Yb ions near 1025 nm is significantly higher than that of other wavebands, which is determined by the luminescence properties of  $\text{Yb}^{3+}$  ions and reabsorption effects. It is challenging for the TSFFLs to obtain consistent laser performances at each operating wavelength. Among the entire tuning range, the 1023-1056 nm waveband has a consistency, including a low ASE and high OSNR, as shown by the enlarged output spectra in Fig. 4(b). These laser peaks also show a highly symmetrical and narrow bandwidth, originating from the nature of the TBF, induced grating, and YCDSF. The laser performances in this waveband will be systematically discussed in the following sections.

To further analyze the lasing properties, the OSNR, the maximum output power, and the slope efficiency of the TSFFL were measured at different working wavelengths. As depicted in Fig. 5(a), the OSNR was above 60 dB at each working wavelength. Among them, the maximum value obtained was 64.34 dB at 1040.45 nm, while the minimum value was 60.15 dB at 1023.82 nm. In Figs. 5(b) and (c), in the entire tuning range, the output power, and slope efficiency are above 37.07 mW and 8.01%, and their maximum values are up to 64.72 mW and 12.21%, respectively. These results indicate that the lasing properties of the laser have some fluctuations, which depend on the gain properties of the YCDSF in this waveband.

The longitudinal-mode characteristics of the TSFFL were assessed using an ESA with a resolution bandwidth of 2 kHz. A 200 MHz acoustic optical modulator (AOM) was used to generate a frequency shift to avoid low-frequency interference. Figure 6(a) presents the measured radio frequency (RF) beating spectra of the 1040.45 nm laser with different pump powers. When the pump power is lower than 680 mW, only one RF signal is observed, which indicates that the laser operates in a SLM. Otherwise, multiple RF signals appear, which shows that the laser operates at the multi-longitudinal mode (MLM) state. This phenomenon may be explained by the following reasons. With the increase of signal optical power, the new ASE pumped by signal light and the refractive index will change slightly. These will affect the working wavelength and bandwidth of the induced grating, and further perturb the stability of the induced grating.

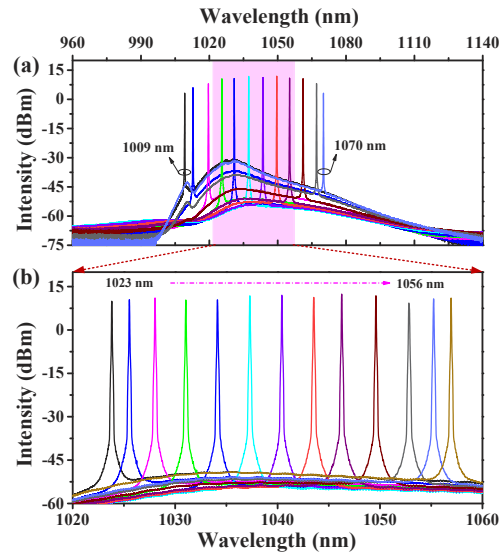


**Fig. 4.** Output spectra of the TSFFL at 1009-1070 nm (a) and 1023-1056 nm (b).

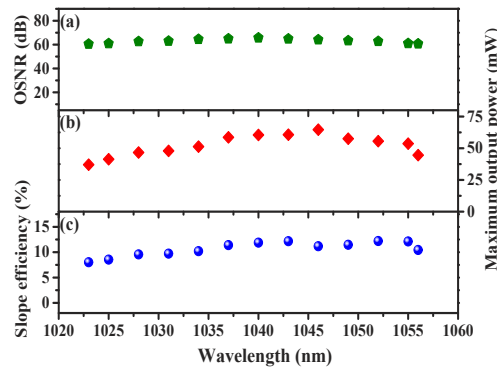


**Fig. 5.** The OSNR (a), maximum output power (b), and slope efficiency (c) of the TSFFL in the wavelength tuning range of 1023 to 1056 nm.

Thus, it cannot effectively suppress the longitudinal mode competition, as also reported in Refs. [15,34,36]. In addition, the pump power was fixed at 680 mW, and the RF signals at different working wavelengths were examined in Fig. 6(b). The results show a prominent signal peak at 200 MHz only, indicating that the laser operates in the SLM in the entire tuning waveband.

Moreover, the linewidths of the TSFFL at different working wavelengths were studied according to the delayed self-heterodyne method. The linewidth measurement system contained a 35-km-long single-mode delay fiber and 200 MHz AOM. At the maximum output power, a series of typical heterodyne signals at different working wavelengths were measured using an ESA with a sweep time of 0.69 s with a bandwidth resolution of 30 Hz, as illustrated in Fig. 7(a). At different operating wavelengths, the signal-to-noise ratio of the heterodyne signal is different, which is caused by the difference in the output properties of the laser. The linewidth of the laser can be estimated by dividing the 20 dB linewidth of the heterodyne signal by 20. The corresponding relationship between the linewidth and working wavelength is also presented in Fig. 7(b). Its linewidth varies from 1.9 to 2.8 kHz, implying that the linewidth is below 2.8 kHz in the entire

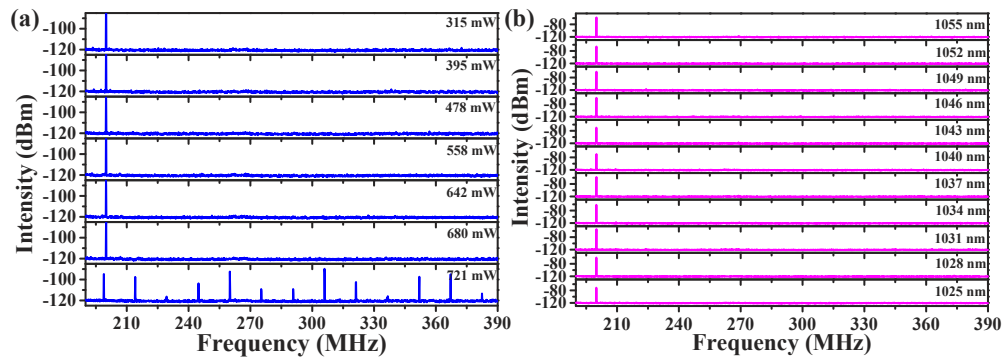


**Fig. 6.** RF beating spectra of the TSFFL with different pump powers (a) and at different working wavelengths (b).

tuning range. The small linewidth fluctuation is mainly caused by the difference in the ASE of the YCDSF and the output power of the TSFFL at different operating wavelengths.

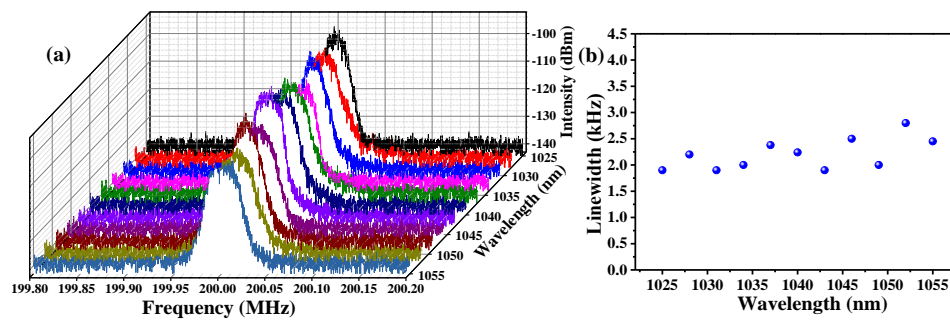


**Fig. 7.** Measured heterodyne signals (a) and linewidths (b) of the TSFFL at different working wavelengths.

The RIN of the laser at 1040.42 nm was examined with different pump powers using an ESA, as depicted in Fig. 8(a). The RIN spectrum at a given pump power is dominated by a sharp peak at the frequency of the relaxation oscillation of the laser. As the pump power increases, the central frequency of the relaxation oscillation peak shifts toward higher frequencies, i.e., from 50.13 kHz at 277 mW to 104.31 MHz at 435 mW, whereas the peak intensity decreases from -134.98 to -141.83 dB/Hz. The RIN stabilized at approximately -155 dB/Hz at frequencies above 1 MHz. No obvious noise peaks were observed. At a pump power of 315 mW, the RIN of the laser at different wavelengths were studied, as shown in Fig. 8(b). With the red shift of the working wavelength, the center frequency of the relaxation oscillation peak initially increased and then decreased, i.e., from 73.80 kHz at 1025.53 nm to 83.14 kHz at 1031.04 nm and then 14.95 kHz at 1055.20 nm. This can be attributed mainly to the small change in cavity length caused by the TBF and the variation in the ratio of the pump power to the threshold with the wavelength [37].

The power stabilities of the TSFFL at six typical working wavelengths were continuously recorded for 100 mins at every 1 s using a PM, as shown in Fig. 9. As the output power of the laser increased, its power fluctuation increased, i.e., from 0.25% at 37.07 mW to 0.38% at 64.70 mW. The small power instability may be attributed to the influence of the pump laser and ambient



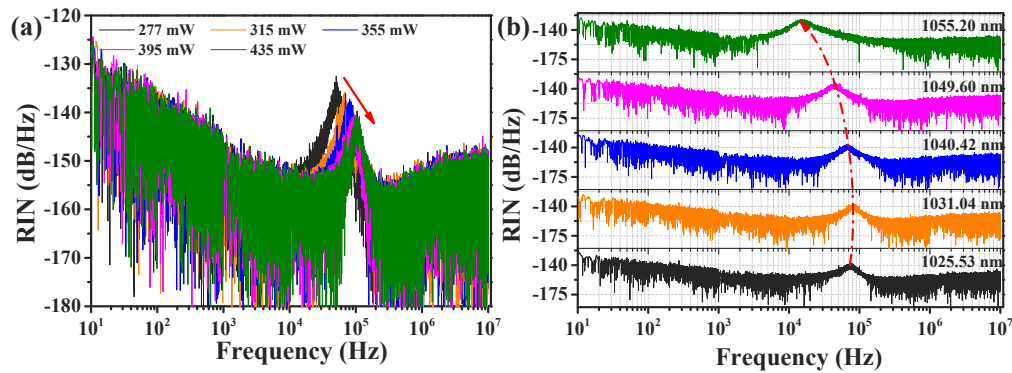


**Fig. 8.** Measured RIN of the TSFFL with different pump powers (a) and at different working wavelengths (b).

temperature. Therefore, the power fluctuation of the TSFFL is below 0.38% across the tuning waveband.

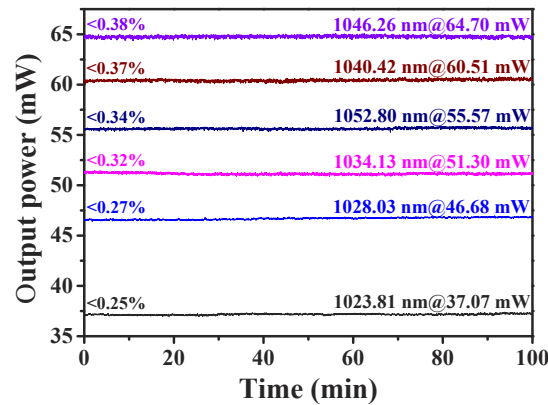


**Fig. 9.** Power stability of the TSFFL at different working wavelengths.

The comparison of the performances of the TSFFLs based on different tunable-SLM-achieved methods are presented in Table 1. The TSFFLs with TBFs have relatively wide wavelength tuning ranges, and most of them possess a range of 60 nm. Their linewidths are very narrow, generally below 10 kHz. The minimum can even reach the order of sub-kHz [31,32]. Compared with TSFFLs with a commercial Yb-doped fiber as a gain fiber [28–33], the TSFFL in this work has two advantages. First, the maximum output power and slope efficiency of the TSFFL based on the YCDSF are doubled (or more than doubled), albeit the utilized length of the YCDSF is only one-sixth (or even one-tenth) of that of the commercial Yb-doped fiber [28,29,33]. This may be due to the high gain coefficient of the YCDSF. The Yb ions doping concentration was 6.57 wt% in YCDSF, and the corresponding gain coefficient in the entire tuning range was above 2 dB/cm, which was higher than that of the commercial Yb-doped fiber. Secondly, the OSNR and RIN are up to 60 dB and lower than -155 dB/Hz, respectively, and are better than those of reported lasers [29,30,33]. This is due to the low ASE noise and no heat accumulation in the laser cavity. TBF with a high OSNR can effectively suppress the ASE of the YCDSF, combined with the absorption effect of the sufficiently long SA fiber, it further weakens the ASE. The YCDSF exhibits good compatibility with commercial silica fibers, indicating no obvious heat accumulation at the

welding point. Furthermore, its power stability was enhanced, owing to the high stability of the induced grating [15]. A sufficiently long induced grating length (4.0 m) improves the stability of the laser. Consequently, the ring-cavity TSFFL based on the homemade YCDSFs and Bi/Er/Yb co-doped fibers has demonstrated an improvement in the laser performance.

**Table 1. Comparison of the TSFFLs based on different methods.**

Methods	TBF+ Multiple-ring cavity					TBF+ Unpumped Yb-doped fiber	
Gain fiber length (cm)	100 <sup>a</sup>	110 <sup>b</sup>	80 <sup>b</sup>	60 <sup>c</sup>	/	100 <sup>a</sup>	13 <sup>d</sup>
Tuning range (nm)	60.0	40.0	60.0	55	84	60.0	61
Maximum output power (mW)	6.0 (dBm)	0.2 (dBm)	20.1	-8.6 (dBm)	9	3.0 (dBm)	64.0
Slope efficiency	/	/	6.8-8.0%	/	/	2.4-4.9%	8.0-12.2%
OSNR (dB)	53	47	50	55	/	50	60-64
Linewidth (kHz)	/	2.38	8.8	0.44	0.6	/	1.9-2.8
RIN (dB/Hz)	/	-135	-140	/	/	/	-155
Power fluctuations	3.6%	0.22dB	1.34%	0.38dB	/	2.3%	<0.38%
Refs	[28]	[29]	[30]	[32]	[31]	[33]	This work

<sup>a</sup>Nufer, SM-YSF-HI,

<sup>b</sup>INO Yb 501,

<sup>c</sup>LIEKKI, Yb1200-4/125,

<sup>d</sup>YCDSF

#### 4. Conclusions

In short, we have demonstrated a homemade high doping concentration YCDSF with 127 nm of the 20 dB ASE spectra bandwidth. The gain coefficient spectra bandwidth of over 2 dB/cm is more than 75 nm. Based on this fiber, over 60 nm SLM laser has been achieved in the range of 1009 to 1070 nm. To the best of our knowledge, this is the first demonstration of a TSFFL in a similar YAG crystal-derived fiber. Especially, a highly consistent laser performance is presented in the 1023-1056 nm waveband. At any working wavelength, the TSFFL had an output power >37 mW with a power fluctuation <0.38%, showing the slope efficiency >8% and an OSNR >60 dB. The linewidths of laser at different working wavelengths were measured, ranging from 1.9 to 2.8 kHz. Their relaxation oscillation frequencies were lower than 110 kHz, and the RIN stabilized at -155 dB/Hz at frequencies above 1.0 MHz. The results show that this broadband high-gain YCDSF is a promising gain medium for constructing low-noise TSFFLs applied in optical coherence tomography, molecular spectroscopy, and so on.

**Funding.** National Key Research and Development Program of China (2020YFB1805800); National Natural Science Foundation of China (61705126, 61735009, 61935002, 61975113); 111 Project (D20031); Shanghai Professional Technical Public Service Platform of Advanced Optical Waveguide Intelligent Manufacturing and Testing (19DZ2294000).

**Disclosures.** The authors declare no conflicts of interest.

**Data availability.** Data underlying the results presented in this paper are not publicly available at this time but may be obtained from the authors upon reasonable request.

#### References

1. Y. C. Huang, Y. K. Lu, J. C. Chen, Y. C. Hsu, Y. M. Huang, S. L. Huang, and W. H. Cheng, "Broadband emission from Cr-doped fibers fabricated by drawing tower," *Opt. Express* **14**(19), 8492–8497 (2006).

2. C. Z. Li, Z. X. Jia, Z. H. Cong, Z. J. Liu, X. Y. Zhang, G. S. Qin, and W. P. Qin, "Gain characteristics of ytterbium-doped SiO<sub>2</sub>-Al<sub>2</sub>O<sub>3</sub>-Y<sub>2</sub>O<sub>3</sub> fibers," *Laser Phys.* **29**(5), 055804 (2019).
3. P. D. Dragic, J. Ballato, T. Hawkins, and P. Foy, "Feasibility study of Yb: YAG-derived silicate fibers with large Yb content as gain media," *Opt. Mater.* **34**(8), 1294–1298 (2012).
4. P. Dragic, P. C. Law, J. Ballato, T. Hawkins, and P. Foy, "Brillouin spectroscopy of YAG-derived optical fibers," *Opt. Express* **18**(10), 10055–10067 (2010).
5. M. Jia, J. X. Wen, X. P. Pan, L. Zhang, J. Yuan, Y. Huang, X. B. Zhang, L. F. He, F. F. Pang, and T. Y. Wang, "Flexible scintillation silica fiber with engineered nanocrystals for remote real-time X-ray detection," *ACS Appl. Mater. Interfaces* **14**(1), 1362–1372 (2022).
6. Y. M. Zhang, G. Q. Qian, X. S. Xiao, X. L. Tian, Z. Chen, J. P. Zhong, Z. J. Ma, and J. R. Qiu, "A yttrium aluminosilicate glass fiber with graded refractive index fabricated by melt-in-tube method," *J. Am. Ceram. Soc.* **101**(4), 1616–1622 (2018).
7. Y. F. Wang, Y. M. Zhang, J. K. Cao, L. P. Wang, X. L. Peng, J. P. Zhong, C. S. Yang, S. H. Xu, Z. M. Yang, and M. Y. Peng, "915 nm all-fiber laser based on novel Nd-doped high alumina and yttria glass@ silica glass hybrid fiber for the pure blue fiber laser," *Opt. Lett.* **44**(9), 2153–2156 (2019).
8. S. P. Zheng, J. Li, C. L. Yu, Q. L. Zhou, L. L. Hu, and D. P. Chen, "Preparation and characterizations of Yb: YAG-derived silica fibers drawn by on-line feeding molten core approach," *Ceram. Int.* **43**(7), 5837–5841 (2017).
9. Y. M. Zhang, W. W. Wang, J. Li, X. S. Xiao, Z. J. Ma, H. T. Guo, G. P. Dong, S. H. Xu, and J. R. Qiu, "Multi-component yttrium aluminosilicate (YAS) fiber prepared by melt-in-tube method for stable single-frequency laser," *J. Am. Ceram. Soc.* **102**(5), jace.16072 (2018).
10. Z. J. Liu, Y. Y. Xie, Z. H. Cong, Z. G. Zhao, Z. X. Jia, C. Z. Li, G. S. Qin, S. Wang, X. B. Gao, X. B. Shao, and X. Y. Zhang, "110 mW single-frequency Yb: YAG crystal-derived silica fiber laser at 1064 nm," *Opt. Lett.* **44**(17), 4307–4310 (2019).
11. Y. Y. Xie, Z. J. Liu, Z. H. Cong, Z. G. Qin, S. Wang, Z. X. Jia, C. Z. Li, G. S. Qin, X. B. Gao, and X. Y. Zhang, "All-fiber-integrated Yb: YAG-derived silica fiber laser generating 6 W output power," *Opt. Express* **27**(3), 3791–3798 (2019).
12. X. B. Gao, Z. H. Cong, Z. G. Zhao, G. S. Qin, Z. X. Jia, Y. Y. Xie, M. Y. Jiang, X. Y. Zhang, and Z. J. Liu, "Single-frequency kHz-linewidth 1070 nm laser based on Yb: YAG derived silica fiber," *IEEE Photonics Technol. Lett.* **32**(14), 895–898 (2020).
13. Y. Wan, J. X. Wen, Y. H. Dong, C. Jiang, M. Jia, F. Z. Tang, N. Chen, Z. W. Zhao, F. F. Pang, and T. Y. Wang, "Exceeding 50% slope efficiency DBR fiber laser based on a Yb-doped crystal-derived silica fiber with high gain per unit length," *Opt. Express* **28**(16), 23771–23783 (2020).
14. Y. Wan, J. X. Wen, C. Jiang, F. Z. Tang, J. Wen, S. J. Huang, F. F. Pang, and T. Y. Wang, "Over 255 mW single-frequency fiber laser with high slope efficiency and power stability based on an ultrashort Yb-doped crystal-derived silica fiber," *Photonics Res.* **9**(5), 649–656 (2021).
15. Y. Wan, J. X. Wen, C. Jiang, K. Zou, F. Z. Tang, F. F. Pang, and T. Y. Wang, "Over 100 mW stable low-noise single-frequency ring-cavity fiber laser based on a saturable absorber of Bi/Er/Yb co-doped silica fiber," *J. Lightwave Technol.* **40**(3), 805–812 (2022).
16. J. Ballato, T. Hawkins, P. Foy, B. Kokuoz, R. Stolen, C. Mcmillen, M. Daw, Z. Su, T. M. Tritt, M. Dubinskii, J. Zhang, T. Sanamyan, and M. J. Matthewson, "On the fabrication of all-glass optical fibers from crystals," *J. Appl. Phys.* **105**(5), 053110 (2009).
17. Y. Y. Xie, Z. H. Cong, Z. G. Zhao, X. Y. Zhang, X. Zhao, W. Zhao, X. B. Shao, and Z. J. Liu, "Preparation of Er: YAG crystal-derived all-glass silica fibers for a 1550-nm single-frequency laser," *J. Lightwave Technol.* **39**(14), 4769–4775 (2021).
18. Y. M. Zhang, G. Q. Tang, X. S. Xiao, X. L. Tian, X. Q. Ding, Z. J. Ma, L. Y. Yang, H. T. Guo, S. H. Xu, Z. M. Yang, and J. R. Qiu, "The preparation of yttrium aluminosilicate (YAS) glass fiber with heavy doping of Tm<sup>3+</sup> from polycrystalline YAG ceramics," *J. Am. Ceram. Soc.* **101**(10), 4627–4633 (2018).
19. G. W. Tang, G. Q. Qian, W. Lin, W. L. Wang, Z. G. Shi, Y. Yang, N. L. Dai, Q. Qian, and Z. M. Yang, "Broadband 2 μm amplified spontaneous emission of Ho/Cr/Tm: YAG crystal derived all-glass fibers for mode-locked fiber laser applications," *Opt. Lett.* **44**(13), 3290–3293 (2019).
20. Y. Wan, J. X. Wen, M. Jia, Z. Liu, Z. W. Zhao, Z. Y. Chen, and T. Y. Wang, "Wide-spectrum properties of Yb: YAG crystal-derived fiber," in *Proceedings of IEEE Conference on International Conference on Optical Communications and Networks* (IEEE, 2019), pp. 1–3.
21. C. Xu and F. W. Wise, "Recent advances in fibre lasers for nonlinear microscopy," *Nat. Photonics* **7**(11), 875–882 (2013).
22. M. Bashkansky, M. D. Duncan, L. Goldberg, J. P. Kopolow, and J. Reintjes, "Characteristics of a Yb-doped superfluorescent fiber source for use in optical coherence tomography," *Opt. Express* **3**(8), 305–310 (1998).
23. R. Royon, J. Lhermite, L. Sarger, and E. Cormier, "High power, continuous-wave ytterbium-doped fiber laser tunable from 976 to 1120 nm," *Opt. Express* **21**(11), 13818–13823 (2013).
24. K. Bultitude, R. Stevens, and P. Ewart, "High-resolution degenerate four-wave-mixing spectroscopy of OH in a flame with a novel single-mode tunable laser," *Appl. Phys. B* **79**(6), 767–773 (2004).
25. H. Al-Taiy, N. Wenzel, S. Preußler, J. Klinger, and T. Schneider, "Ultra-narrow linewidth, stable and tunable laser source for optical communication systems and spectroscopy," *Opt. Lett.* **39**(20), 5826–5829 (2014).

26. M. Siddiqui, A. S. Nam, S. Tozburun, N. Lippok, C. Blatter, and B. J. Vakoc, "High-speed optical coherence tomography by circular interferometric ranging," *Nat. Photonics* **12**(2), 111–116 (2018).
27. F. Wellmann, M. Steinke, F. Meylahn, N. Bode, B. Willke, L. Overmeyer, J. Neumann, and D. Kracht, "High power, single-frequency, monolithic fiber amplifier for the next generation of gravitational wave detectors," *Opt. Express* **27**(20), 28523–28533 (2019).
28. F. F. Yin, S. G. Yang, H. W. Chen, M. H. Chen, and S. Z. Xie, "60-nm-wide tunable single-longitudinal mode ytterbium fiber laser with passive multiple-ring cavity," *IEEE Photonics Technol. Lett.* **23**(22), 1658–1660 (2011).
29. K. L. Wang, B. L. Lu, X. Y. Qi, Z. R. Wen, K. L. Zhang, H. W. Chen, and J. T. Bai, "Wavelength-tunable single-frequency ytterbium-doped fiber laser based on a double-circulator interferometer," *Laser Phys. Lett.* **16**(1), 015104 (2019).
30. B. L. Lu, J. Kang, X. Y. Qi, X. Q. Feng, L. Hou, M. Jiang, H. W. Chen, Y. Wang, K. L. Wang, and J. T. Bai, "High-stability broadband wavelength-tunable single-frequency ytterbium-doped all-fiber compound ring cavity," *IEEE Photonics J.* **9**(2), 1–8 (2017).
31. P. Honzatko, Y. Baravets, and A. K. Myakalwar, "Single-frequency fiber laser based on a fiber ring resonator filter tunable in a broad range from 1023 nm to 1107 nm," *Opt. Lett.* **43**(6), 1339–1342 (2018).
32. K. L. Wang, B. L. Lu, Z. R. Wen, X. Y. Qi, J. Y. Ding, H. W. Chen, and J. T. Bai, "Widely tunable ytterbium-doped single-frequency all-fiber laser," *Opt. Laser Technol.* **128**, 106242 (2020).
33. F. F. Yin, S. G. Yang, H. W. Chen, M. H. Chen, and S. Z. Xie, "Tunable single-longitudinal-mode Ytterbium all fiber laser with saturable-absorber-based auto-tracking filter," *Opt. Commun.* **285**(10-11), 2702–2706 (2012).
34. Z. H. Sun, X. T. Jiang, Q. Wen, W. J. Li, and H. Zhang, "Single frequency fiber laser based on an ultrathin metal-organic framework," *J. Mater. Chem. C* **7**(16), 4662–4666 (2019).
35. Z. M. Sathi, J. Z. Zhang, Y. H. Luo, J. Canning, and G. D. Peng, "Improving broadband emission within Bi/Er doped silicate fibres with Yb co-doping," *Opt. Mater. Express* **5**(10), 2096–2105 (2015).
36. R. Poozesh, K. Madanipour, and P. Parvin, "High SNR watt-level single frequency Yb-doped fiber laser based on a saturable absorber filter in a cladding-pumped ring cavity," *J. Lightwave Technol.* **36**(20), 4880–4886 (2018).
37. L. H. Huang, C. S. Yang, T. Y. Tan, W. Lin, Z. T. Zhang, K. J. Zhou, Q. L. Zhao, X. D. Teng, S. H. Xu, and Z. M. Yang, "Sub-kHz-linewidth wavelength-tunable single-frequency ring-cavity fiber laser for C-and L-band operation," *J. Lightwave Technol.* **39**(14), 4794–4799 (2021).